Cellular automata in photonic cavity arrays

Li, Jing; Liew, Timothy Chi Hin

2016

Li, J., & Liew, T. C. H. (2016). Cellular automata in photonic cavity arrays. Optics Express, 24(22), 24930-.

https://hdl.handle.net/10356/85895

https://doi.org/10.1364/OE.24.024930

Research Article | Vol. 24, No. 22 | 31 Oct 2016 | OPTICS EXPRESS 24930

Optics EXPRESS

Cellular automata in photonic cavity arrays

JING LI AND T. C. H. LIEW*

Division of Physics and Applied Physics, School of Physical and Mathematical Sciences, Nanyang Technological University, 21 Nanyang Link, 637371, Singapore

*tchliew@gmail.com

Abstract: We propose theoretically a photonic Turing machine based on cellular automata in arrays of nonlinear cavities coupled with artificial gauge fields. The state of the system is recorded making use of the bistability of driven cavities, in which losses are fully compensated by an external continuous drive. The sequential update of the automaton layers is achieved automatically, by the local switching of bistable states, without requiring any additional synchronization or temporal control.

OCIS codes: (190.0190) Nonlinear optics; (200.4560) Optical data processing; (160.5298) Photonic crystals.

References and links

1. V. R. Almedia, C. A. Barrios, R. R. Panepucci, and M. Lipson, "All-optical control of light on a silicon chip," Nature **431**, 1081–1084 (2004).
2. I. Carusotto and C. Ciuti, "Quantum fluids of light," Rev. Mod. Phys. **85**, 299–374 (2013).
3. C. Leyder, T. C. H. Liew, A. V. Kavokin, I. A. Shelykh, M. Romanelli, J. Ph. Karr, E. Giacobino, and A. Bramati, "Interference of Coherent Polariton Beams in Microcavities: Polarization-Controlled Optical Gates," Phys. Rev. Lett. **99**, 196402 (2007).
4. C. Adrados, T. C. H. Liew, A. Amo, M. D. Martín, D. Sanvitto, C. Antón, E. Giacobino, A. Kavokin, A. Bramati, and L. Viña, "Motion of Spin Polariton Bullets in Semiconductor Microcavities," Phys. Rev. Lett. **107**, 146402 (2011).
5. M. De Giorgi, D. Ballarini, E. Cancellieri, F. M. Marchetti, M. H. Szymanska, C. Tejedor, R. Cingolani, E. Giacobino, A. Bramati, G. Gigli, and D. Sanvitto, "Control and Ultrafast Dynamics of a Two-Fluid Polariton Switch," Phys. Rev. Lett. **109**, 266407 (2012).
6. E. Cancellieri, J. K. Chana, M. Sich, D. N. Krizhanovskii, M. S. Skolnick, and D. M. Whittaker, "Logic gates with bright dissipative polariton solitons in Bragg cavity systems," Phys. Rev. B **92**, 174528 (2015).
7. D. Ballarini, M. De Giorgi, E. Cancellieri, R. Houdré, E. Giacobino, R. Cingolani, A. Bramati, G. Gigli, and D. Sanvitto, "All-optical polariton transistor," Nature Comm. **4**, 1778 (2013).
8. T. Gao, P. S. Eldridge, T. C. H. Liew, S. I. Tsintzos, G. Stavrinidis, G. Deligeorgis, Z. Hatzopoulos, and P. G. Savvidis, "Polariton condensate transistor switch," Phys. Rev. B **85**, 235102 (2012).
9. R. Cerna, Y. Léger, T. K. Paraïso, M. Wouters, F. Morier-Genoud, M. T. Portella-Oberli, and B. Deveaud, "Ultrafast tristable spin memory of a coherent polariton gas," Nature Comm. **4**, 2008 (2013).
10. G. Christmann, C. Coulson, J. J. Baumberg, N. T. Pelekanos, Z. Hatzopoulos, S. I. Tsintzos, and P. G. Savvidis, "Control of polariton scattering in resonant-tunneling double-quantum-well semiconductor microcavities," Phys. Rev. B **82**, 113308 (2010).
11. M. Amthor, T. C. H. Liew, C. Metzger, S. Brodbeck, L. Worschech, M. Kamp, I. A. Shelykh, A. V. Kavokin, C. Schneider, and S. Höfling, "Optical bistability in electrically driven polariton condensates," Phys. Rev. B **91**, 081404 (2015).
12. R. P. Feynman, "Simulating Physics with Computers," Int. J. Theor. Phys. **21**, 467–488, (1982).
13. S. Wolfram, "Computation Theory of of Cellular Automata," Commun. Math. Phys. **96**, 15–57 (1984).
14. I. Karafyllidis, "Design of a dedicated parallel processor for the prediction of forest fire spreading using cellular automata and genetic algorithms," Eng. Appl. Artif. Intell. **17**, 19–36, (2004).
15. M. A. Arbib, "Simple self-reproducing universal automata," Inf. Control **9**, 177-189, (1966).
16. Ch. Mizas, G. Ch. Sirakoulis, V. Mardiris, I. Karafyllidis, N. Glykos, and R. Sandaltzopoulos, "Reconstruction of DNA sequences using genetic algorithms and cellular automata: Towards mutation prediction?" BioSystems **92**, 61–68, (2008).
17. L. Nalpantidis, A. Amanatiadis, G. Ch. Sirakoulis, A. Gasteratos, "Efficient hierarchical matching algorithm for processing uncalibrated stereo vision images and its hardware architecture," IET Image Process. **5**, 481–492, (2011).
18. S. A Chatzichristofis, D. A Mitzias, G. Ch. Sirakoulis, Y. S Boutalis, "A novel cellular automata based technique for visual multimedia content encryption," Opt. Commun. **283**, 4250–4260, (2010).
19. I. Karafyllidis, "Cellular quantum computer architecture," Phys. Lett. A **320**, 35–38, (2003).
20. I. Karafyllidis, "Definition and evolution of quantum cellular automata with two qubits per cell," Phys. Rev. A **70**, 044301 (2004).

#270851 http://dx.doi.org/10.1364/OE.24.024930
Journal © 2016 Received 20 Jul 2016; revised 15 Sep 2016; accepted 16 Sep 2016; published 17 Oct 2016

Optics EXPRESS

21. S. Wolfram, "Statistical mechanics of cellular automata," Rev. Mod. Phys. **55**, 601–644 (1983).
22. M. Cook, "Universality in Elementary Cellular Automata Complex Systems," Complex Systems **15**, 1 (2004).
23. X. Zhang, Y. Wang, J. Sun, D. Liu, and D. Huang, "All-optical AND gate at 10 Gbit/s based on cascaded single-port-couple SOAs," Opt. Express **12**, 361-366 (2004).
24. Z. J. Li, Z. W. Chen, and B. J. Li, "Optical pulse controlled all-optical logic gates in SiGe/Si multimode interference," Opt. Express **13**, 1033–1038 (2005).
25. P. Andalib, and J. Granpayeh, "All-optical ultracompact photonic crystal AND gate based on nonlinear ring resonators," J. Opt. Soc. Am. B **26**, 10–16 (2009).
26. Y. Liu, F. Qin, Z. M. Meng, F. Zhou, Q. H. Mao, and Z. Y. Li, "All-optical logic gates based on two-dimensional low-refractive-index nonlinear photonic crystal slabs," Opt. Express **19**, 1945-1953 (2011).
27. M. Ghadrdan, and M. A. Mansouri-Birjandi, "All-Optical NOT Logic Gate Based on Photonic Crystals," Int. J. Electr. Comput. Eng. (LJECE) **3**, 478–482 (2013).
28. W. P. Lin, Y. F. Hsu, and H. L. Kuo, "Design of Optical Nor Logic Gates Using Two Dimension Photonic Crystals," Am. J. Mod. Phys. **2**, 144–147 (2013).
29. A. Baas, J. Ph. Karr, H. Eleuch, and E. Giacobino, "Optical bistability in semiconductor microcavities," Phys. Rev. A **69**, 023809 (2014).
30. N. A. Gippius, S. G. Tikhodeev, V. D. Kulakovskii, D. N. Krizhanovskii and A. I. Tartakovskii, "Nonlinear dynamics of polariton scattering in semiconductor microcavity: Bistability vs. stimulated scattering," Europhys. Lett. **67**, 997–1003 (2004).
31. D. M. Whittaker, "Effects of polariton-energy renormalization in the microcavity optical parametric oscillator," Phys. Rev. B **71**, 115301 (2005).
32. H. Ohadi, Y. del Valle-Inclan Redondo, A. Dreismann, Y. G. Rubo, F. Pinsker, S. I. Tsintzos, Z. Hatzopoulos, P. G. Savvidis, and J. J. Baumberg, "Tunable Magnetic Alignment between Trapped Exciton-Polariton Condensates," Phys. Rev. Lett. **116**, 106403 (2016).
33. R. O. Umucalilar, and I. Carusotto, "Artificial gauge field for photons in coupled cavity arrays," Phys. Rev. A **84**, 043804 (2011).
34. T. K. Paraiso, M. Wouters, Y. Leger, F. Morier-Genoud, and B. Deveaud-Pledran, "Multi-stability of a coherent spin ensemble in a semiconductor microcavity," Nature Mater. **9**, 655–660 (2010).
35. B. Nelsen, Gangqiang Liu, M. Steger, D. W. Snoke, R. Balili, K. West, and L. Pfeiffer, "Dissipationless Flow and Sharp Threshold of a Polariton Condensate with Long Lifetime," Phys Rev. X **3**, 041015 (2013).
36. A. Dreismann, H. Ohadi, YVI Redondo, R. Balili, Y. G. Rubo, S. I. Tsintzos, G. Deligeorgis, Z. Hatzopoulos, P. G. Savvidis, and J. J. Baumberg, "A sub-femtojoule electrical spin-switch based on optically trapped polariton condensates," Nature Mater. advanced online publication at doi: 10.1038/nmat4722 (2016).
37. V. Savona, and W. Langbein, "Realistic heterointerface model for excitonic states in growth-interrupted GaAs quantum wells," Phys. Rev. B **74**, 075311 (2006).
38. T. C. H. Liew, Yuri G. Rubo, and A. V. Kavokin, "Generation and Dynamics of Vortex Lattices in Coherent Exciton-Polariton Fields," Phys. Rev. Lett. **101**, 187401 (2008).
39. T. Espinosa-Ortega, T. C. H. Liew, and I. A. Shelykh, "Optical diode based on exciton-polaritons," Appl. Phys. Lett. **103**, 191110 (2013).

1. Introduction

Optical information processing is promising due to its low-loss propagation and low heating, which can potentially lead to high operation speed with reduced error checking requirements. A requirement for optical computing and data processing is an efficient interaction among different optical modes, which typically depends on strong material nonlinearities. Nonlinear coefficients in conventional materials are generally small, leading to high power requirements for optical gates. Nonlinearity can be enhanced by confining light in resonating structures like microring resonators [1] or microcavities [2]. In the latter structures, strong coupling with excitons in quantum wells was shown to give rise to highly nonlinear exciton-polariton modes, which have allowed various implementations of individual logic gates [3–6] and transistors [7, 8]. As significant improvements continue, including low-power ultrafast switching [9] and interfacing with electronics [10, 11], an outstanding question in polaritonics remains as to how individual processing elements can be combined and scaled to yield complete information processing systems. This requires both a scheme of universal logic and a mechanism of cascading multiple elements [7].

Cellular automata (CAs) are well-known for generating complex global behaviour from simple local rules. They are an interesting platform for studying the boundary between stability

Optics EXPRESS

and chaos. Prior and more recent works demonstrated that CAs are very effective in simulating physical systems and solving scientific problems, because they can capture the essential features of systems where global behaviour emerges from the collective effect of simple components which interact locally [12, 13]. During the last two decades, there have been an extensive variety of one-dimensional (1-D) CA applications to be proposed on several scientific fields like: simulation of physical systems [14], biological modelling involving models for self-reproduction [15], biological structures and DNA sequences [16], image processing [17], cryptography [18], etc. In addition, CAs developed to model quantum systems are referred to as quantum cellular automata (QCAs), and the evolution of QCAs with two qubits per cell has been widely studied by Karafyllidis using a quantum computer simulator [19,20]. There are $2^3 = 8$ possible configurations for a cell and its two immediate neighbors. The rule defining 1D cellular automaton must specify the resulting state for each of these possibilities so there are $256 = 2^{2^3}$ possible elementary cellular automata, while many of these rules are trivially equivalent to each other up to a simple transformation of the underlying geometry. Among the 88 possible unique elementary cellular automata, Rule 110 is the only one for which Turing completeness has been proven [21, 22]. Thus, the introduction of an automaton architecture can replace the need for logic gates, which are typically sought in optical information processing systems such as those based on photonic crystals [23–28]. We focus on the simplest known Turing complete system Rule 110 cellular automaton (often simply Rule 110), which can be represented with a layered set of cells, each of which may exist in one of two states. The configuration of each layer is determined sequentially, where each cell has its state determined by the state of the three nearest cells in the preceding layer. The rule 110 automaton is thus characterized by the response of each cell to the 8 possible combinations of these three cells, which is given in Table 1.

Table 1. Definition of the rule 110 automaton in terms of responses to different input configurations:

Input cell states:	111	110	101	100	011	010	001	000
Output cell state:	0	1	1	0	1	1	1	0

In this paper, we point out that the rule 110 cellular automaton can be realized with a coupled set of cavities, corresponding to an array of nonlinear photonic crystal cavities or an array of coupled polariton boxes in a single microcavity structure. To provide a robust definition of binary logic states we make use of the phenomenon of optical (polariton) bistability in microcavities [29–31], driven by a near-resonant laser. The strong nonlinear interactions between polaritons have been shown to allow low optical energy (pico joule) switching between bistable states on ultrafast (picosecond) timescales [9]. Furthermore, despite losses in the system the state of each cavity is highly robust, being maintained so long as the continuous wave laser drive is applied. At the same time, the state of each cavity can be influenced by neighbouring cavities [32]. Treating each cavity as a cell of an automaton, we show that the rule 110 can be reproduced provided the couplings between different cavities have specific phases to engineer specific interferences capable of switching the bistable state under the correct configurations. Phase dependent coupling in cavity arrays was previously introduced in [33] in the form of controllable artificial gauge fields. Due to the Turing completeness associated with the automaton, this is one of few universal schemes of (classical) computation based on exciton-polaritons in microcavities and in principle offers a scalable solution.

Optics EXPRESS

2. Theoretical model

We begin with the Bose-Hubbard Hamiltonian describing a coupled array of cavities:

$$\mathcal{H} = \sum_i \left(-\Delta \hat{a}_i^\dagger \hat{a}_i + \alpha \hat{a}_i^\dagger \hat{a}_i\right) + \sum_{\langle i,j\rangle} J_{ij} \hat{a}^\dagger \hat{a} e^{-i\theta_{ij}} + F \frac{1}{1+e^{-\frac{t-t_0}{\tau_0}}} \left(\hat{a}_i^\dagger + \hat{a}_i\right) + \sqrt{P_i}\, e^{-\frac{(t-t_1)^2}{\tau_1^2}} \left(\hat{a}_i^\dagger + \hat{a}_i\right) \quad (1)$$

where $\hat{a}_i$ is the field operator for cavity i, written in the frame rotating at the frequency of laser excitation, with F the amplitudes of laser excitation of each cavity. We assume that all cavities experience the same amplitude, frequency and phase of laser drive, which is formed uniformly for all cavities at time t_0 over duration τ_0. P_i is a pumping pulse applied to the selected cavities to excite a particular state at time t_1 (τ_1 defines the pulse duration). Δ is the energy detuning between the laser energy and cavity mode energy; α is the strength of local (intra-cavity) Kerr nonlinearity; J_{ij} represents a fixed coupling between cavities. We allow for an associated phase with the coupling between different cavities, θ_{ij}, which could be introduced following the techniques in [33]. The above Bose-Hubbard Hamiltonian is applicable to a wide-variety of systems, including coupled arrays of nonlinear photonic crystals as well as polariton microcavities (in which case $\hat{a}_i$ can be interpreted as the polariton field operator).

We will work in the classical regime. Adding a standard Lindblad form dissipation term, the evolution of the field operators can be derived from the corresponding master equation. Applying the mean-field approximation, $\langle \hat{a}_i \rangle = \psi_i$, gives the nonlinear Schrödinger (Gross-Pitaevskii) equation describing the coupled cavity array:

$$i\hbar \frac{d\psi_i}{dt} = \left(-\Delta + \alpha|\psi_i|^2 - i\Gamma\right)\psi_i + F \frac{1}{1+e^{-\frac{t-t_0}{\tau_0}}} + \sum_j J_{ij}\psi_j e^{-i\theta_{ij}} + \sqrt{P_i}\, e^{-\frac{(t-t_1)^2}{\tau_1^2}} \quad (2)$$

where Γ is the decay rate. The topology of the cavity array described by J_{ij} is shown in Fig. 1(a).

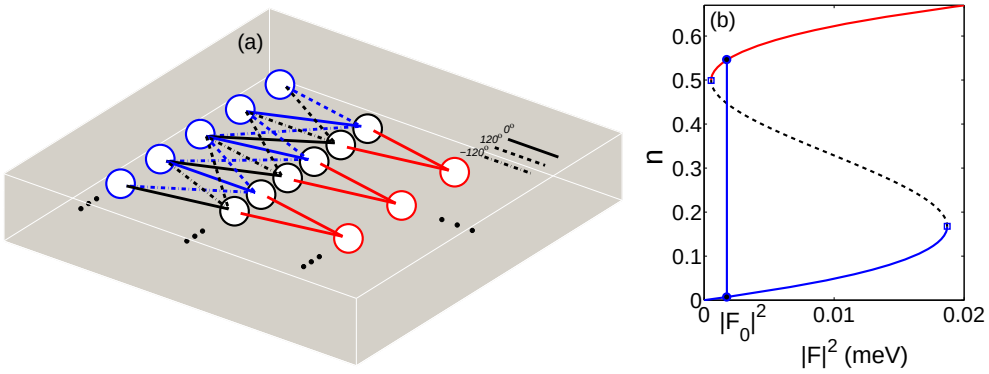

Fig. 1. (a) Architecture of cavity array. Color solid circles show cavities in layers corresponding to the automaton cells, while black circles correspond to an auxiliary layer of cavities used to reproduce the 110 rule. Different strengths of connections between cavities are marked with different line styles. (b) Dependence of the intensity of a single uncoupled cavity on pump power. The S-shaped curve is characteristic of a bistable system: the lower (blue) and the upper (red) branches include the possible states; the dashed line indicates unstable states. The vertical line indicates a selected pump intensity for which the cavity intensity can be switched between its two stable values. Parameters: $\Delta = 0.5\,meV$ and $\Gamma = \hbar/20$ meV.

Optics EXPRESS

This particular array represents a layered automaton, in which the state of the cavities represented by red solid circles is dependent on the layer of cavities represented by blue solid circles. An auxiliary layer of cavities, represented by black solid circles, is introduced between these layers. As we will show, this layer allows reproduction of the 110 rule between the layers represented by solid circles with colors.

For a single cavity, with no coupling to neighbours, the stationary states (in the limit of time independent excitation) of Eq. (2) are given analytically by [29–31]:

$$|F|^2 = \left[(\alpha n_s - \Delta)^2 + \Gamma^2\right] n_s \tag{3}$$

where $n_s = |\psi_s|^2$ defines the stationary intensity. If the pump energy is tuned above the bare cavity/polariton mode energy by an amount $\Delta > \sqrt{3}\Gamma$, then the system demonstrates bistability, which is characterized by an S-shaped response of the intensity n_s to the laser intensity $|F|^2$ as shown in Fig. 1(b). If the pump intensity is increased from zero, the polariton intensity increases steadily from zero until reaching a stable point on the lower branch of the S-shaped curve. If an additional pulse P_i is applied then the total pump intensity effectively increases instantaneously and changes the state to that on the upper branch of the S-shaped curve. The power requirements for running an automaton with the proposed scheme are defined by the power needed to observe bistability of the individual cavity modes. In semiconductor mesa microcavities of 3 micron diameter, bistability has been reported consuming 50 W/cm^2 some time ago [34]. Since then, the polariton lifetime has been improved by two orders of magnitude [35]. While bistability was not studied in these most modern samples, given that power requirements scale inversely with the cube of the lifetime, one can expect sub nanowatt power consumption per mesa. Given that the calculation time scales with the automaton size, the total energy consumption of an automaton routine would scale with the square of the number of cells in the input layer. Very recent work has also demonstrated particularly low sub-femtojoule energy consumption in electrically driven exciton-polariton condensates [36].

3. Realization of Rule 110

The switching of the state of a cavity due to coupling with its neighbours can be understood by seeing that the last term in Eq. (2) effectively changes the driving amplitude from F to $F + \sum_j J_{ij}\psi_j e^{-i\theta_{ij}}$. If the intensity of this effective driving exceeds the upper threshold calculated in Fig. 1(b) for the single cavity, then the cavity automaton state will be switched from low to high intensity. Note that the effective driving intensity depends on the state of the connected cavities through their amplitudes ψ_j and the interference of these amplitudes in the sum, which depends on the coupling strengths J_{ij} and coupling phases θ_{ij}.

To realize a cellular automaton we consider the case where F is chosen such that all cavities exhibit bistability. The state of the automaton is initialized by preparing the state of the cavities in the first layer either in low or high intensity states, representing 0 and 1 in Table 1. All other cavities are initially in the low intensity, 0 state.

Each triplet of cavities in the first automaton layer are coupled to two cavities in the first auxiliary layer. The purpose of these two cavities is to realize different parts of the 110 rule. In particular, the first auxiliary cavity should switch on if the input state of the triplet of cavities is 110, 011 or 010, while the second auxiliary cavity should switch on if the input state of the triplet of cavities is 001, 011, or 101. This behaviour can be realized for specific choices of J_{ij} and ϕ_{ij}. To see this we can consider first the addition of terms in the effective driving of the first auxiliary cavity: $F + J_1\psi_1 e^{-i\theta_1} + J_2\psi_2 e^{-i\theta_2} + J_3\psi_3 e^{-i\theta_3}$, where it should be understood that ψ_1, ψ_2 and ψ_3 refer to the amplitudes of the first three cavities in the first automaton layer. The couplings J_1, J_2 and J_3, together with phases θ_1, θ_2, and θ_3 correspond to coupling from these first three cavities to the first auxiliary cavity.

Optics EXPRESS

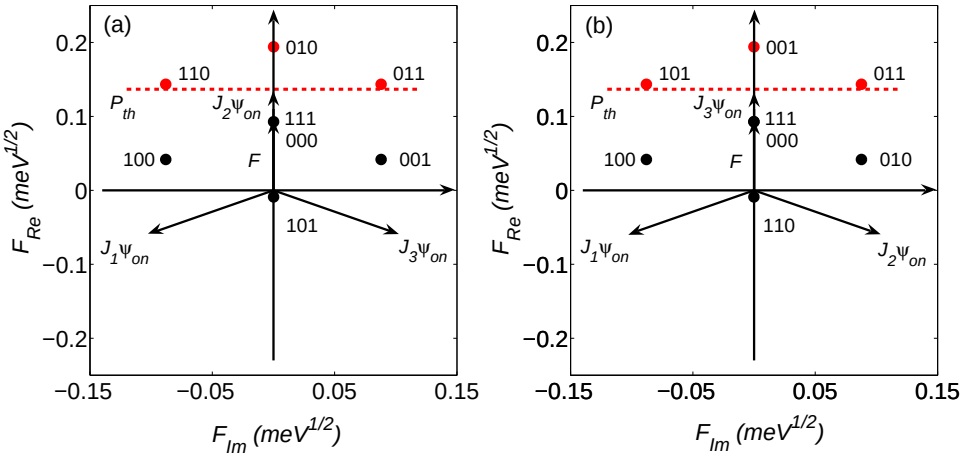

Fig. 2. The phasor diagram showing how the direct driving term F and coupling terms from neighbouring cavities $J_1\psi_1 e^{-i\theta_1}$, $J_2\psi_2 e^{-i\theta_2}$, and $J_3\psi_3 e^{-i\theta_3}$ interfere to generate an effective driving. The dashed line shows the threshold corresponding to the second turning point in Fig. 1(b). If the effective drive exceeds this value, then a cavity will be switched. a) Example of interference causing triplets of cavities in states 110, 011 or 011 to switch on an auxiliary cavity. b) Example of interference causing triplets of cavities in states 001, 011 or 101 to switch on an auxiliary cavity. Parameters: $|J_1| = |J_2| = |J_3| = 0.1015$. (a) $\theta_2 = 0°$, $\theta_1 = -120°$, and $\theta_3 = 120°$. (b) $\theta_1 = -120°$, $\theta_2 = 120°$, $\theta_3 = 0°$.

An example with a particular choice of values of couplings and phases is shown in the phasor diagram in Fig. 2(a), which shows how different terms interfere to generate the effective driving. Since different terms have different phases they must be added vectorially in the phasor diagram. The terms to add also depend on the initial state of the three first cavities in the first automaton layer. Only if a cavity is initiated in the high intensity state does it contribute significantly to the effective driving of the auxiliary cavity. The different points in the phasor diagram show the result of the interference and consequent effective driving for different possible configurations in the first layer. The horizontal dashed line shows the threshold for switching. Consequently, we see that the auxiliary cavity switches if the three cavities feeding it have states 010, 011, or 110.

Figure. 2(b) considers now the coupling of triplets of cavities in the first layer to the second auxiliary cavity. Using a slightly different choice of phases we find that the second auxiliary cavity switches when the three cavities feeding it have states 001, 011, or 101.

To complete the rule 110 we now consider the coupling of the auxiliary cavity states to the next automaton layer. It is straightforward to choose the coupling strengths such that if either auxiliary cavity has been switched then it switches the cavity to which it couples in the next layer into the high intensity state. Consequently the state of a cavity in the layer following the auxiliary cavity layer can be switched depending on the state of its nearest three cavities in the layer preceding the auxiliary layer according to the 110 rule. The results in Fig. 3 demonstrate how the state of a cavity switches according to the 110 rule. Furthermore, to simulate disorder, we tested our scheme adding random constants to the values of Δ in Eq. (2) of each cavity. We found that for a root mean squared value of disorder of 0.1 *meV*, the scheme continues to function. This is a typical value of disorder in semiconductor microcavities [37, 38].

It is worth noting that the reason that the 110 rule automaton is capable of computationally non-trivial tasks is because it represents a nonlinear cut in the input state space. In Fig. 2 we have used different coupling phases to separate the input states in phasor space. The threshold

Optics EXPRESS

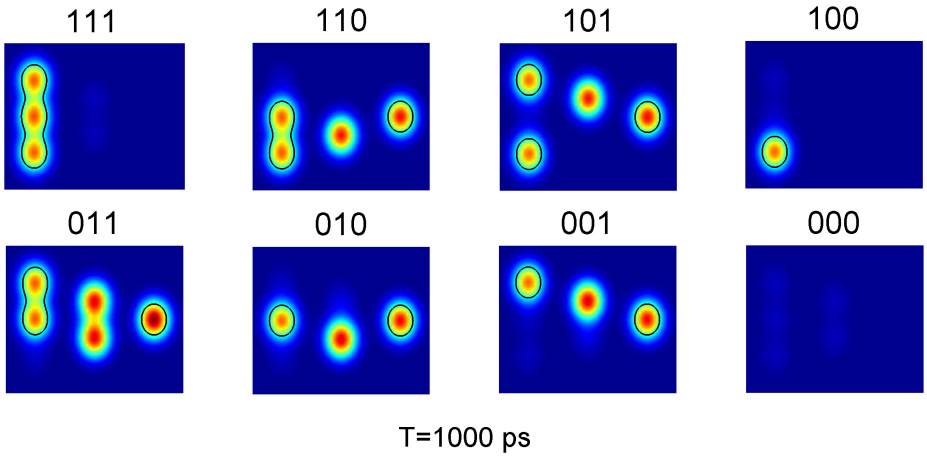

Fig. 3. Intensities of coupled automaton cavities after the state of the cavities in the first layer (left-most cavities) has been set to a particular configuration. The state of the final cavity (right-most) is switched to its higher intensity according to the 110 rule (Table 1).

mechanism of bistability introduces a linear cut in this space (given by the horizontal dashed line), but it is unable to make a nonlinear cut where all states activated by the 110 rule can simultaneously be above threshold. For this reason, two auxiliary cavities are needed to realize different cuts in the phasor space. The combination of states in the auxiliary cavities is then able to reproduce the 110 rule.

In the above analysis we have considered only the forward coupling between layers in the network and neglected any effect of switching in any particular layer to a previous layer. Feedback suppression could also be archived by using optical diodes to couple cavities unidirectionally. Diode schemes compatible with bistability have been proposed theoretically by patterning the shape of the polariton potential [39].

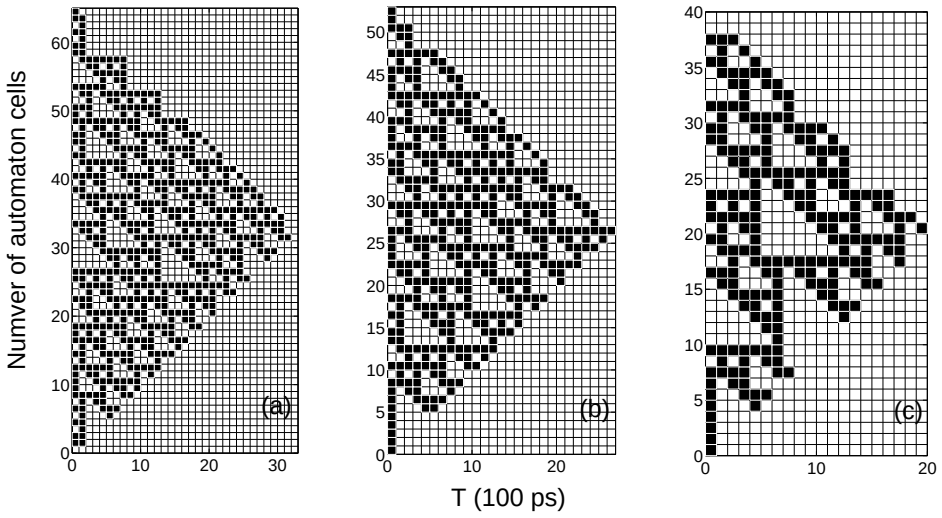

Fig. 4. Multi-layer cavity array with different numbers (65, 53, 40) of automaton cells for (a), (b) and (c), respectively.

Optics EXPRESS

4. Numerical results

To demonstrate the rule 110 automaton, we now consider a complete cavity array described by Eq. (2). We initiate the states of the cavities in the first layer either in the low intensity 0 state or high intensity 1 state corresponding to the bistable curve by applying the laser pulse P_i to some of the automaton cells in the first layer. The coupling between triplets of cavities in the first layer and the auxiliary cavities significantly increase the effective driving of the auxiliary cavity, then the auxiliary cavity has been switched, and also the state of the next layer cavity was switched due to the coupling of the auxiliary cavity states to the next automaton layer. Fig. 4 shows the resulting final state of all cavities in the system, which illustrates how self-replicating structures characteristic of cellular automata are generated.

5. Conclusions

We introduced the concept of cellular automata using coupled arrays of bistable resonators, which could be realized with exciton-polaritons in semiconductor microcavities, for example. By engineering the interference between coupled cavities it is possible to realize the cellular automaton defined by the 110 rule. This is confirmed with numerical simulations using the nonlinear Schrödinger equation to represent the dynamics of the system. The automaton based on the 110 rule falls into the class of Turing complete automata, thus the system in principal represents a complete scheme of optical based information processing. In theory the system is fully scalable and can be implemented with a single microcavity or photonic crystal structure. The use of bistability allows for the robust maintenance of binary states, where losses are conveniently compensated by a continuous laser drive.